Supplementary Materials

Enhancing the activity and stability of RuO_2-based catalyst *via* nano-confinement effect for O_2 evolution reaction in acid electrolyte

Shukai Liu[1,2], Huang Tan[3], Gaole Dai[2], Shiyun Xiong[3], Yu Zhao[2], Benxia Li[1]

[1]School of Chemistry and Chemical Engineering, Key Laboratory of Surface & Interface Science of Polymer Materials of Zhejiang Province, Zhejiang Sci-Tech University, Hangzhou 310018, Zhejiang, China.
[2]College of Materials, Chemistry and Chemical Engineering, Key Laboratory of Organosilicon Chemistry and Material Technology (Ministry of Education), Hangzhou Normal University, Hangzhou 311121, Zhejiang, China.
[3]School of Materials and Energy, Guangzhou Key Laboratory of Low-Dimensional Materials and Energy Storage Devices, Guangdong University of Technology, Guangzhou 510006, Guangdong, China.

***Correspondence to:** Prof. Benxia Li, School of Chemistry and Chemical Engineering, Key Laboratory of Surface & Interface Science of Polymer Materials of Zhejiang Province, Zhejiang Sci-Tech University, 928 Second Avenue, Hangzhou 310018, Zhejiang, China. E-mail: libx@zstu.edu.cn; Prof. Yu Zhao, College of Materials, Chemistry and Chemical Engineering, Key Laboratory of Organosilicon Chemistry and Material Technology (Ministry of Education), Hangzhou Normal University, 2318 Yuhangtang Rd., Hangzhou 311121, Zhejiang, China. E-mail: yuzhao@hznu.edu.cn

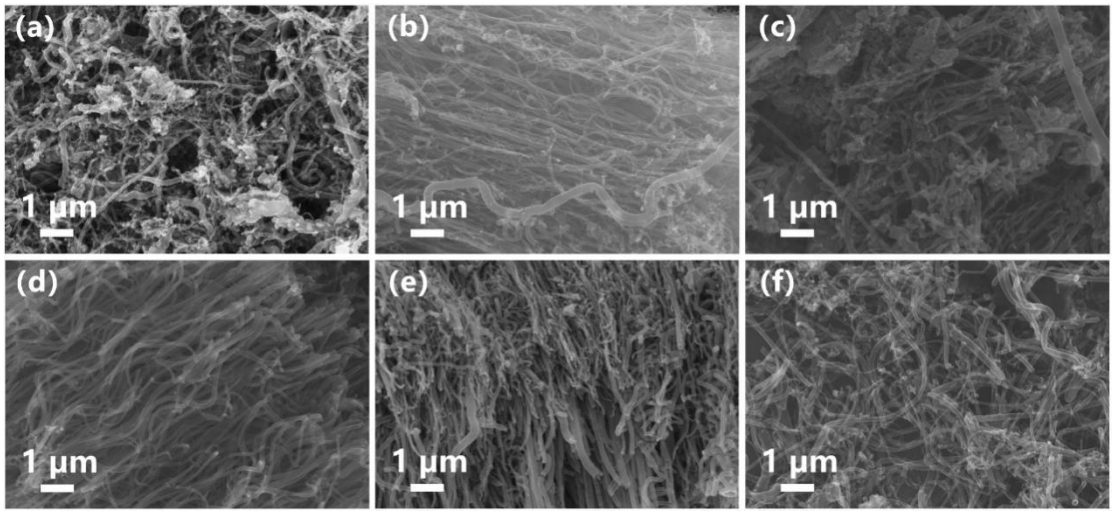

Figure S1. SEM images of CNTs synthesized with different EtOH: ACN ratios as carbon sources: (a) 5:0; (b) 4:1; (c) 3:2; (d) 2:3; (e) 1:4; (f) 0:5.

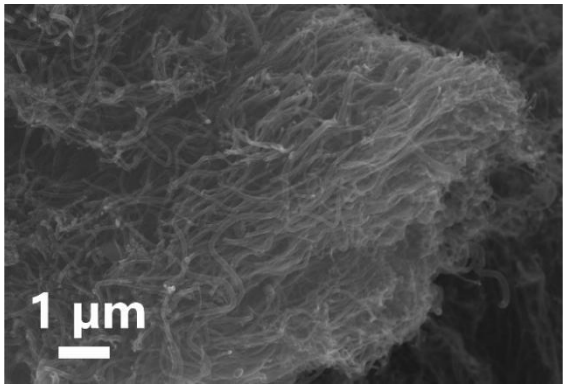

Figure S2. SEM image of CNT/Fe-Ni.

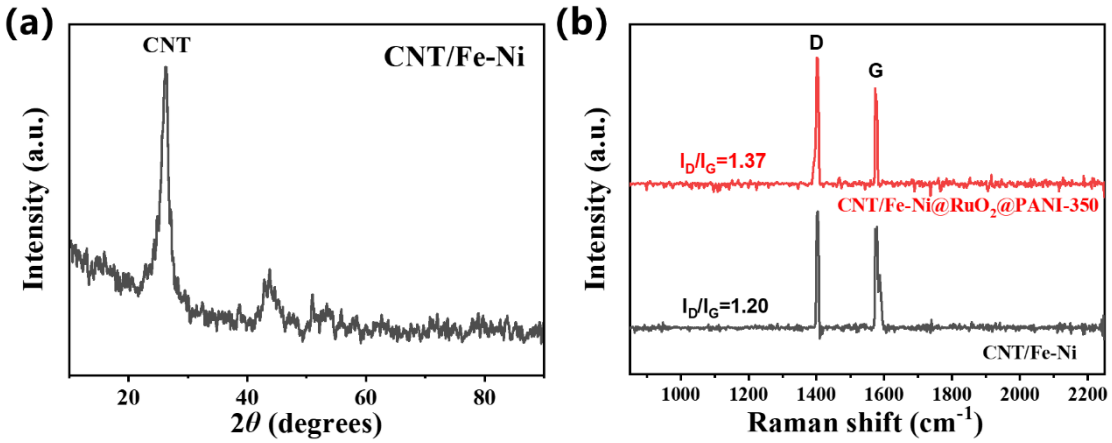

Figure S3. (a) XRD pattern of the CNT/Fe-Ni sample, (b) Raman spectra of both CNT/Fe-Ni and CNT/Fe-Ni@RuO_2@PANI-350 samples.

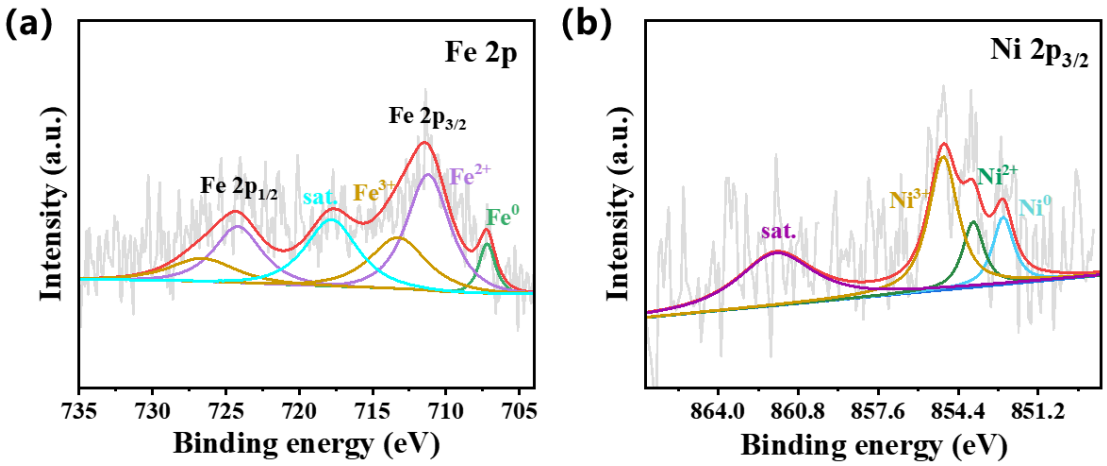

Figure S4. XPS spectra of CNT/Fe-Ni: a) Fe 2p, b) Ni $2p_{3/2}$。

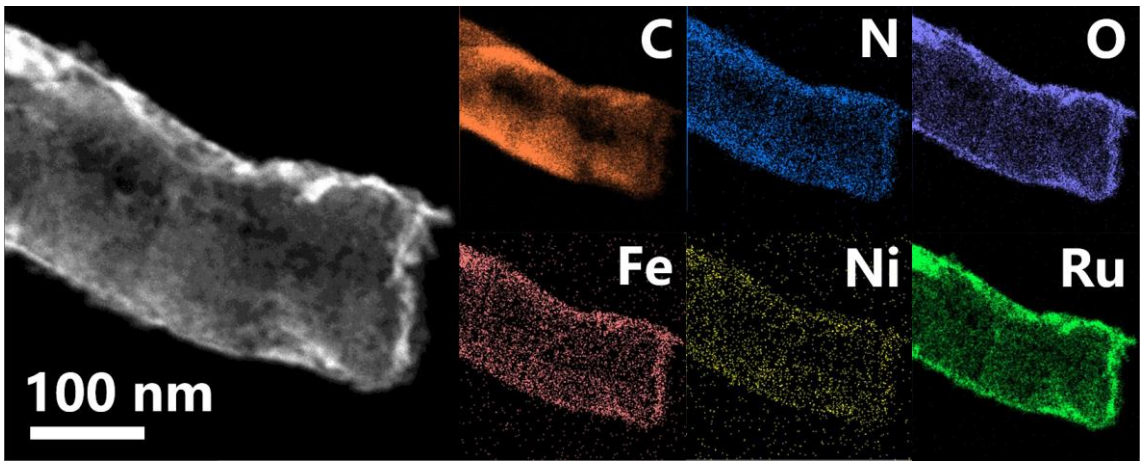

Figure S5. STEM and elemental mapping images of the CNT/Fe-Ni@RuO_2@PANI-350 catalyst.

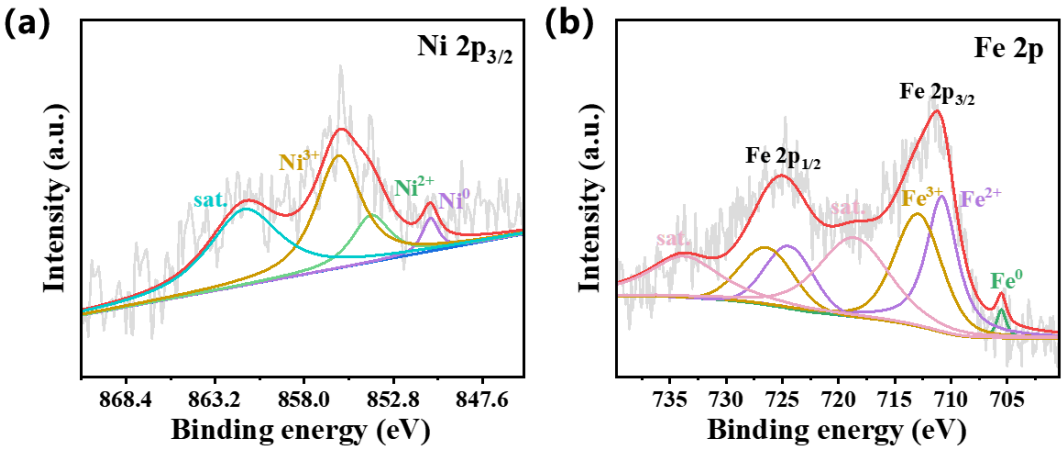

Figure S6. XPS spectra of CNT/Fe-Ni@RuO_2@PANI-350: a) Ni $2p_{3/2}$, b) Fe 2p。

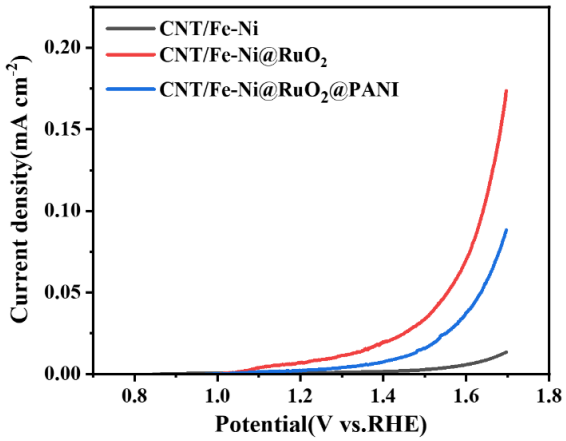

Figure S7. OER catalytic performance of different catalysts in 0.5 M H_2SO_4 solution.

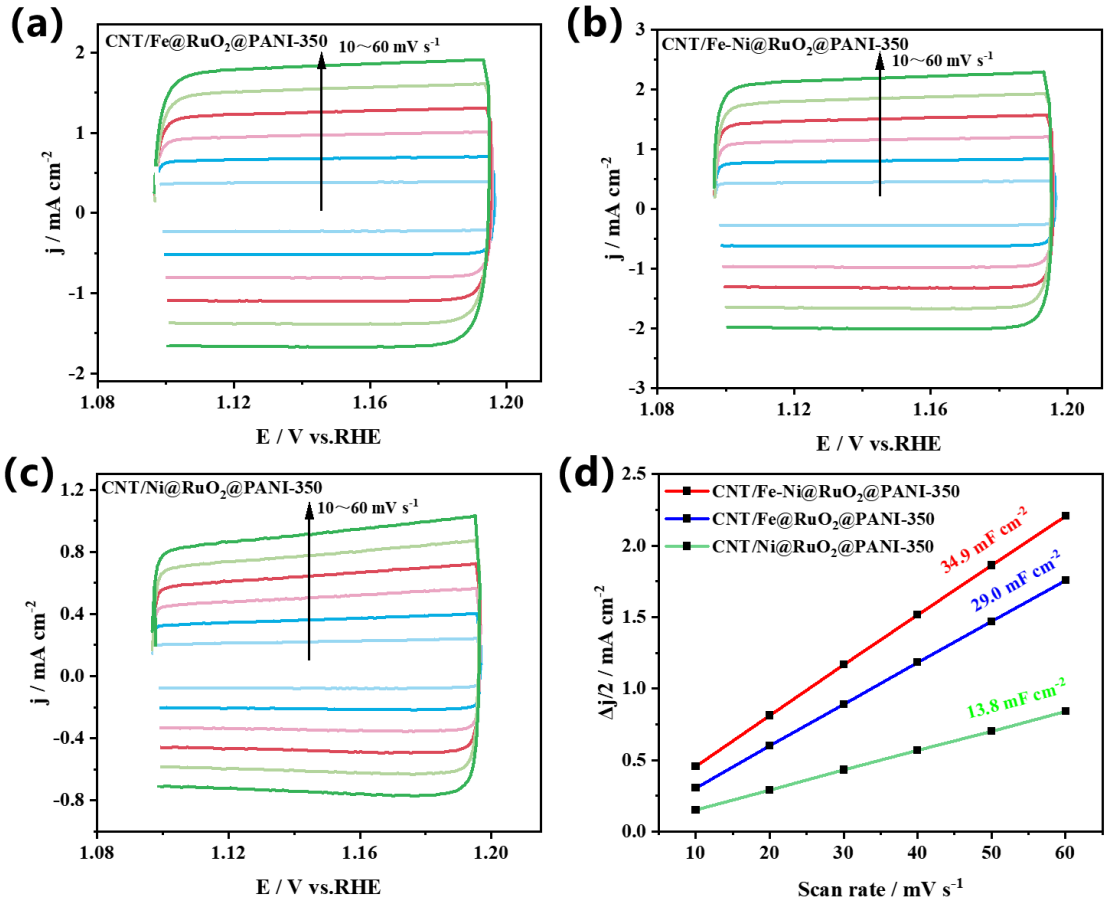

Figure S8. a) CV curves of CNT/Fe@RuO_2@PANI-350, b) CNT/Fe-Ni@RuO_2@PANI-350, c) CNT/Ni@RuO_2@PANI-350 in 0.5 M H_2SO_4 at different scan rates ranging from 10 to 60 mV s^{-1} within the potential range of 1.1–1.2 V vs. RHE, d) the relationship between $\triangle J/2$ and scan rate (v) at 1.15 V, where the slope represents the C_{dl} value of the catalyst.

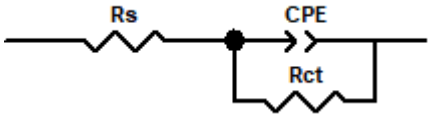

Figure S9. Simplified Randles equivalent circuit used for electrochemical impedance spectroscopy (EIS) measurements.

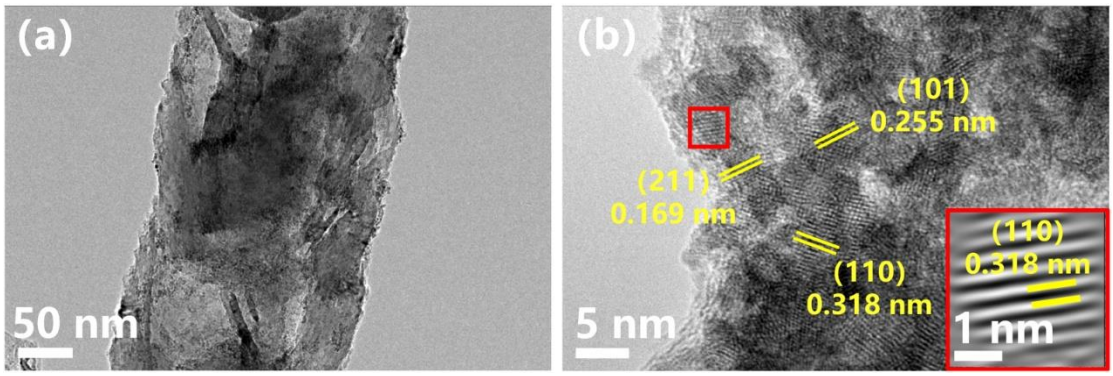

Figure S10. (a) TEM and (b) HRTEM images of CNT/Fe-Ni@RuO_2@PANI-350 after 150 h of OER in 0.5 M H_2SO_4 (the inset is the corresponding in-FFT image).

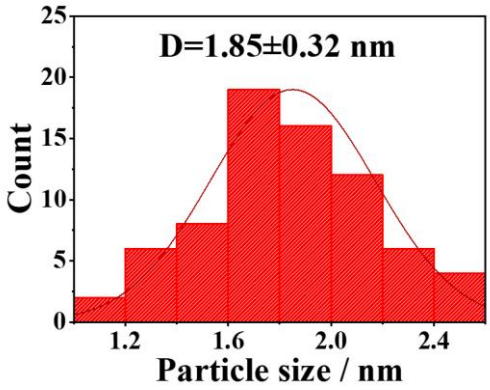

Figure S11. Particle size distribution histogram of RuO_2 nanoparticles for the CNT/Fe-Ni@RuO_2@PANI-350 catalyst after 150 h OER testing

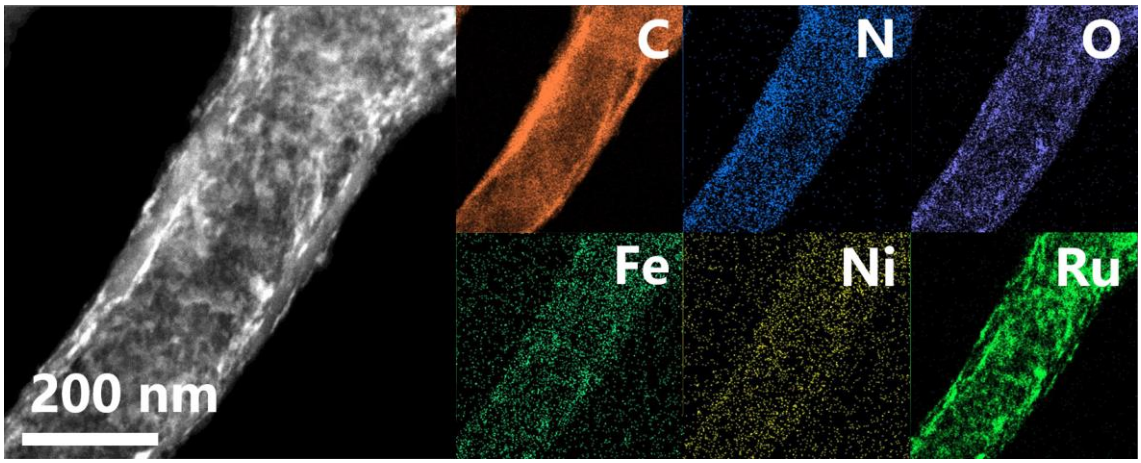

Figure S12. STEM and elemental mapping images of CNT/Fe-Ni@RuO_2@PANI-350 after the OER reaction in 0.5 M H_2SO_4 electrolyte.

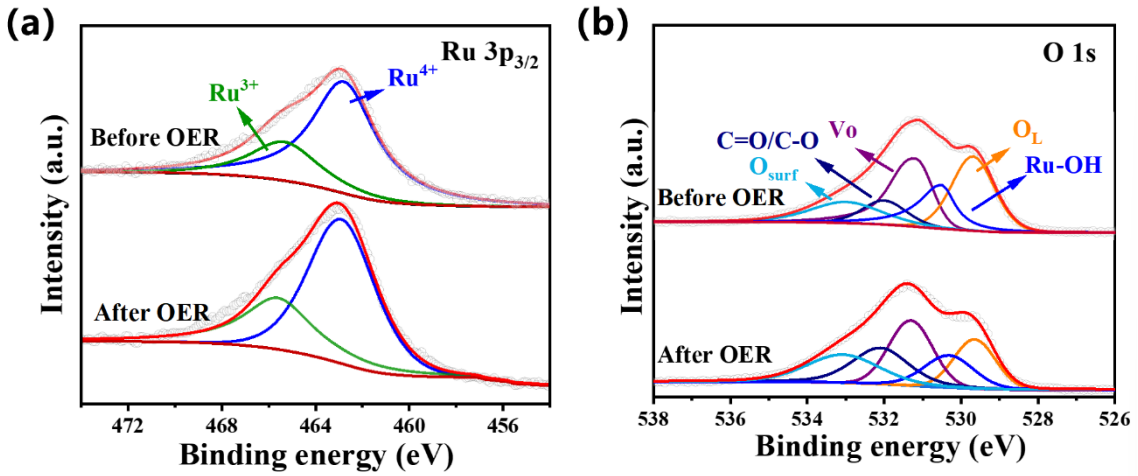

Figure S13. XPS spectra of (a) Ru 3p and (b) O 1s for the CNT/Fe-Ni@RuO_2@PANI-350 catalyst before and after 150 hours of the electrocatalytic OER process at 10 mA cm^{-2}.

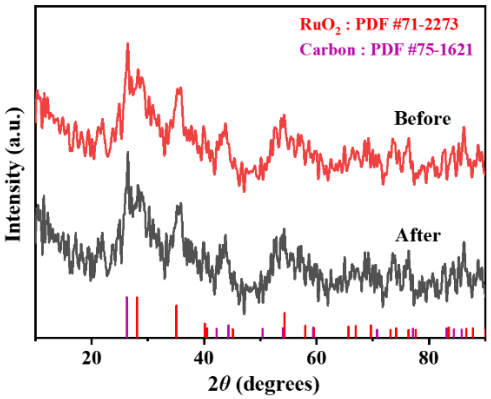

Figure S14. XRD patterns of CNT/Fe-Ni@RuO_2@PANI-350 before and after 150 hours of the electrocatalytic OER process at 10 mA cm^{-2}.

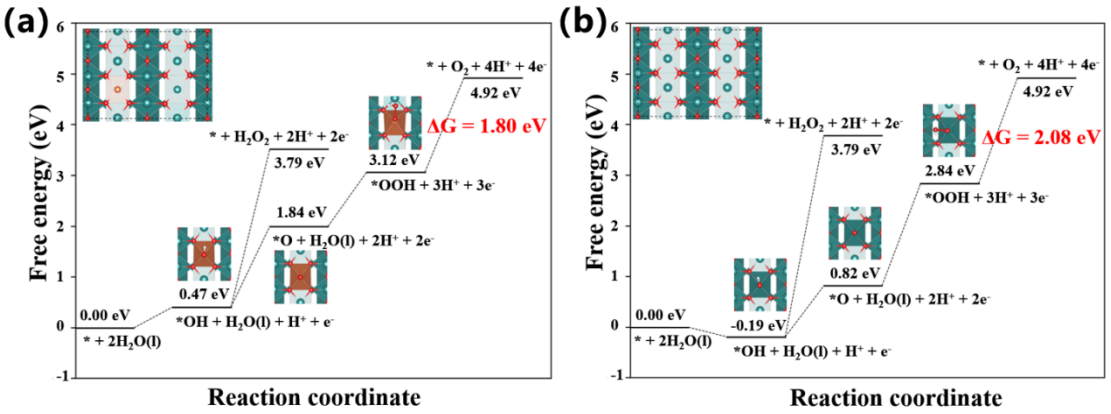

Figure S15. OER free energy diagrams of (a) GPE/Fe@RuO_2 and (b) GPE@RuO_2.

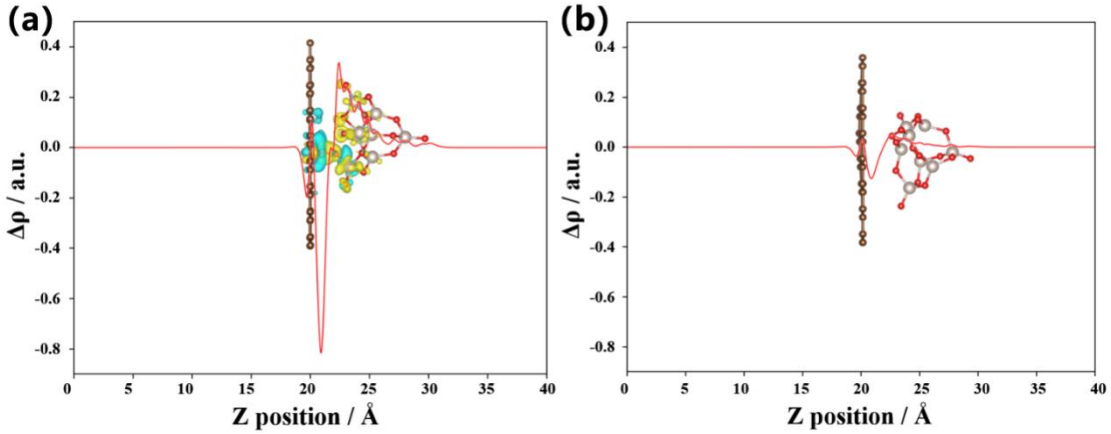

Figure S16. Differential charge density analysis of (a) GPE/Fe@RuO_2 and (b) GPE@RuO_2.

Table S1. The percentages of RuO_2, CNT, Fe-Ni alloy, and PANI in CNT/Fe-Ni@RuO_2@PANI-350 calculated from XPS analysis.

RuO_2 wt%	CNT wt%	Fe-Ni alloy wt%	PANI wt%
40.7	44.6	0.4	7.6

Table S2. Comparison of the performance of CNT/Fe-Ni@RuO_2@PANI-350 with reported catalysts in acidic electrolytes.

Catalyst	Electrolyte	η_{10} (mV)	Tafel Plots (mV dec^{-1})	Rct (Ω)	Stability (10 mA cm^{-2})	Ref.
CNT/Fe-Ni@RuO_2@PANI-350	0.5 M H_2SO_4	188	39.1	31.8	150 h(30 mV overpotential increase)	This Work
$Bi_{0.15}Ru_{0.85}O_2$	0.5 M H_2SO_4	200	59.6	-	100 h	[1]
Co-RuO_2/TiO_2	0.5 M H_2SO_4	266	65.0	53.1	50 h	[2]
$La_{0.1}Ru_{0.9}O_2$	0.5 M H_2SO_4	188	76.6	-	63 h	[3]
RuOxSey-800	0.5 M H_2SO_4	211	45.4	-	18 h	[4]
Si-RuO_x@C	0.5 M H_2SO_4	220	53.0	-	100 h	[5]
$Co_{0.25}Ru_2O_{7-\delta}$	0.5 M H_2SO_4	275	61.0	-	~20 h	[6]
IrPdRhMoW/C	0.5 M H_2SO_4	188	35.0	-	100 h	[7]
Pd@RuO_2	0.5 M H_2SO_4	189	65.2	42.26	100 h	[8]
$Mn_{0.2}Ru_{0.8}O_2$	0.5 M H_2SO_4	214	40.8	-	50 h	[9]
$(Y_{0.2}Ho_{0.2}Dy_{0.2}Gd_{0.2}Pr_{0.2})_2Ru_2O_7$	0.5 M H_2SO_4	200	42.6	-	50 h	[10]
C-RuO_2-RuSe-10	0.5 M H_2SO_4	212	50.4	-	50 h	[11]
E–Zn–RuO_2	0.5 M H_2SO_4	190	50.9	-	60 h	[12]
B-RuO_2	0.5 M H_2SO_4	200	55.0	-	12 h	[13]
PtCo-RuO_2/C	0.5 M H_2SO_4	212	48.5	-	20 h	[14]

References

[1] u, L.; Liang, Q.; Zhao, J.; et al. A Bi-doped RuO_2 catalyst for efficient and durable acidic water oxidation. *Chin. J. Catal.* **2023**, *55*, 182-190. DOI: 10.1016/s1872-2067(23)64554-1

[2] Lu, L.; Xu, Z.; Wei, S.; et al. Dopant-induced electronic state modulation of ruthenium oxide for enhanced acidic oxygen evolution reaction. *Chem. Eng. J.* **2024**, *500*, 157107. DOI: 10.1016/j.cej.2024.157107

[3] Li, C. H.; Yuan, C. Z.; Huang, X.; et al. Tailoring the electron redistribution of RuO_2 by constructing a Ru-O-La asymmetric configuration for efficient acidic oxygen evolution. *eScience* **2024**, *5*, 2667-1417. DOI: 10.1016/j.esci.2024.100307

[4] Du, P.; Lin, C.; He, X.; et al. Controlled fabrication of Ru-O-Se composites for enhanced acidic oxygen evolution. *Adv. Compos. Hybrid Mater.* **2023**, *6*:40. DOI: 10.1007/s42114-023-00624-5

[5] Liu, C.; Jiang, Y.; Wang, T.; et al. Nano Si-Doped Ruthenium Oxide Particles from Caged Precursors for High-Performance Acidic Oxygen Evolution. *Adv. Sci.* **2023**, *10*, 2207429. DOI: 10.1002/advs.202207429

[6] Han, N.; Feng, S.; Liang, Y.; et al. Achieving Efficient Electrocatalytic Oxygen Evolution in Acidic Media on Yttrium Ruthenate Pyrochlore through Cobalt Incorporation. *Adv. Funct. Mater.* **2023**, *33*, 2208399. DOI: 10.1002/adfm.202208399

[7] Zhang, D.; Shi, Y.; Chen, X.; et al. High-entropy alloy metallene for highly efficient overall water splitting in acidic media, *Chin. J. Catal.* **2023**, *45*, 174-183. DOI: 10.1016/s1872-2067(22)64166-4

[8] ao, T.; Jiao, D.; Wang, L.; et al. Switchable Acidic Oxygen Evolution Mechanisms on Atomic Skin of Ruthenium Metallene Oxides. *J. Am. Chem. Soc.* **2025**, *147*, 4159-4166. DOI: 10.1021/jacs.4c13656

[9] un, H.; Kang, E.; Moon, J.; et al. Quantity effect of heteroatom incorporation on the oxygen evolution mechanism in ruthenium oxide. *Chem.* **2024**, *11*, 2451-9294. DOI: 10.1016/j.chempr.2024.11.005

[10] Zhang, J.; Shi, L.; Miao, X.; et al. A new-type high-entropy electrocatalyst with a pyrochlore structure for acid-water oxidation. *J. Mater. Chem. A.* **2024**, *12*, 12785-12794. DOI: 10.1039/d4ta01382d

[11] Wang, J.; Cheng, C.; Yuan, Q.; et al. Exceptionally active and stable RuO_2 with interstitial carbon for water oxidation in acid. Chem. **2022**, *8*, 1673-1687. DOI: 10.1016/j.chempr.2022.02.003

[12] Zhou, Y. N.; Yu, N.; Lv, Q. X.; et al. Surface evolution of Zn doped-RuO_2 under different etching methods towards acidic oxygen evolution. *J. Mater. Chem. A.* **2022**, *10*, 16193-16203. DOI: 10.1039/d2ta03527h

[13] Liu, C.; Sheng, B.; Zhou, Q.; et al. Motivating Ru-bri site of RuO_2 by boron doping toward high performance acidic and neutral oxygen evolution. *Nano Res.* **2022**, *15*, 7008-7015. DOI: 10.1007/s12274-022-4337-z

[14] Jin, H.; Choi, S.; Bang, G. J. Safeguarding the RuO_2 phase against lattice oxygen oxidation during acidic water electrooxidation. *Energy Environ. Sci.*, **2022**, *15*, 1119-1130. DOI: 10.1039/D1EE02636D